LANGMUIR

pubs.acs.org/Langmuir

Article

Cracking of Colloidal Films to Generate Rectangular Fragments

Yunchan Lee, Jaekyoung Kim, Soojin Lee, Sanghyuk Wooh, Hyunsik Yoon,* and Kookheon Char*

Cite This: *Langmuir* 2022, 38, 4935−4941

Read Online

ACCESS | Metrics & More | Article Recommendations | Supporting Information

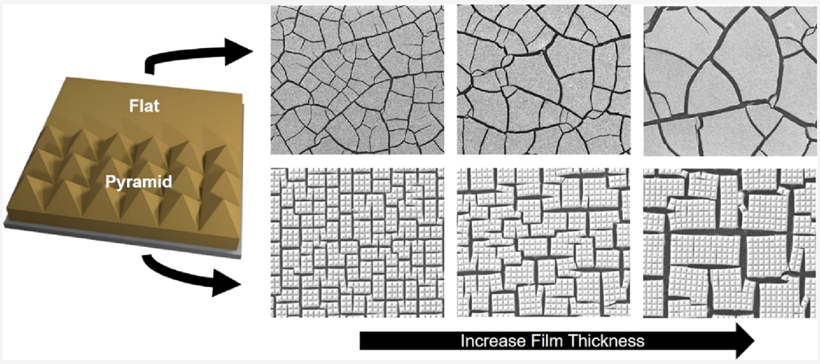

ABSTRACT: Cracks are common in nature. Cracking is known as an irreversible and uncontrollable process. To control the cracking patterns, many researchers have proposed methods to prepare notches for stress localization on films. In this work, we investigate a method of controlling cracks by making microscale pyramid patterns that have notches between the pyramids. After preparing pyramid patterns consisting of colloidal particles with organic residue, we annealed them to induce volume shrinkage and cracking between the pyramids. We studied the effect of film thickness on cracking and the generation of rectangular fragments consisting of multiple pyramids. The area of rectangular fragments was in good agreement with the results of scaling analysis. The concept of controlling cracks by imprinting notches on a film and the relationship with the film thickness can guide the study of cracking phenomena.

■ INTRODUCTION

Cracks can be found in mud, paint, ceramics, and skin.[1−4] They generally produce irregular forms by releasing stresses originating from volume shrinkage during the drying process.[5,6] Recently, the control of the crack formation has received attention because it can be used for device applications such as ultrasensitive sensors inspired by the spider's sensory system or membrane electrode assemblies for high-performance fuel cells.[7,8] Many studies have been conducted to understand crack mechanisms[9−12] and control crack shapes[13,14] or patterns.[15−17] Irregular fragments have their own patterns, such as spiral cracks, and are functions of the film thickness,[18−21] humidity,[22] and volatility of the liquid[23] in cracks formed during drying. To control the crack generation, the guidance of crack formation by using prepatterned surfaces, notches, or applying lateral tensile stress to an elastomeric substrate coated with thin metal films has been reported.[7,8,24−28] Among the methods, the notch effect showed the highest controllability to generate cracks by stress localization because it can be used as an initiation point for cracks. Notches have been prepared by microfabrication, coating colloidal films on patterned substrates and imprinting notches on colloidal films. In particular, we demonstrated cracking at tapered edges between pyramids to prepare microscale pyramidal particles in the previous work.[28] The relationship between the film thickness and the cracked area or the spacing between fragments[5,19,29] has been studied experimentally,[30−32] theoretically,[29,33] and by simulations.[34] This relationship can be used to predict paint film thicknesses in ancient paintings[35] or to understand desiccation patterns in sessile blood drops.[36,37]

In this work, we investigate the effect of notches and film thicknesses by imprinting pyramidal shapes on colloidal films. We used a soft imprinting method on a wet TiO_2 paste to form microscale pyramids in a film.[28,38] After calcination steps, which eliminated all the organic compounds in the TiO_2 films, crack-induced fragments were generated by tensile stress due to volume shrinkage. When the film thickness is thin, there is no cracking in the film because the stress did not sufficiently accumulate. As the film thickness increases, the stress localization can work to generate cracks, and it depends on

Received: February 9, 2022
Revised: March 23, 2022
Published: April 11, 2022

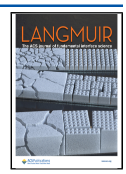

https://doi.org/10.1021/acs.langmuir.2c00328
Langmuir 2022, 38, 4935−4941

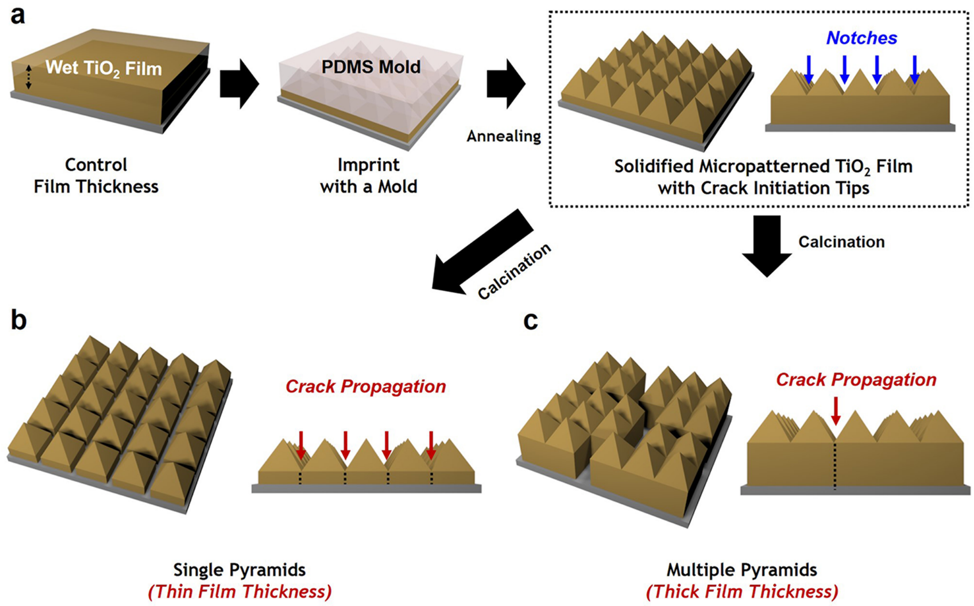

Figure 1. (a) Schematic illustration of controlled crack manipulation by the soft molding of pyramidal structures. (b) Single pyramids isolated after cracking when the residual thickness is thin (~12 μm), and (c) multiple pyramids isolated after cracking when the residual thickness is thick (~34 μm).

the notches and the size of the microscale pyramids. When the film thickness is much higher, the accumulated stress is much higher than the localized stress on the notches prepared by soft imprinting. By using pyramidal shapes, we can generate rectangular fragments, and the size of the fragments depends on the film thickness. We analyzed the relationship between the fragment sizes and the film thickness by using the scaling theory, and the results showed good agreement with and without the pyramid patterns. The formation of rectangular fragments by cracking films with pyramid patterns can guide a new analysis method to study cracking phenomena.

■ METHODS

Fabrication of Patterned PDMS Molds. Pyramid patterned master molds prepared using a micromachining technique were used as the basic molds. The homogeneous mixtures of the multifunctional acrylated prepolymer and acrylate-functionalized polysiloxane (PUA, MINS 301 RM) were poured onto the master mold, and a short ultraviolet (UV) exposure (~10 s) was applied through transparent poly(ethylene terephthalate) films to prepare replica molds. The precured PUA replica was carefully detached from the master mold, and a post-UV treatment was applied for 2 h to fully cure the PUA surface. The polydimethylsiloxane (PDMS) (Sylgard 184 silicon elastomer, Dow Corning) prepolymer mixture with a weight ratio of 10:1 (precursor/curing agent) was poured onto the PUA replica master and thermally cured at 80 °C for 6 h. After full curing, the PDMS was cut into patterns to obtain each mold.

Fabrication of TiO_2 Flat Films with Different Thicknesses. A paste composed of 20 nm TiO_2 was purchased from Dyesol (DSL 18NR-T). A wet, flat, thin film was fabricated by the doctor blade coating method, and two different spacers (Kapton tape for 35 μm and Scotch tape for 60 μm) were used to control the thickness. To make a uniformly thick film, we introduced a method of layering thin films one-by-one. A thin film was coated using one spacer and annealed at 60 °C for 90 min to evaporate approximately 40 wt % of the solvent to solidify the film. Then, the same procedure was repeated by increasing the number of spacers one-by-one. The TiO_2 film thickness was controlled by the number of spacers.

Fabrication of Crack Initiation Notches and Cracking in TiO_2 Films. A PDMS mold with a pyramid pattern was stamped onto a wet film and detached after drying at 60 °C for 30 min. The film was sintered at 500 °C for 20 min with a controlled heating rate (10 °C/min) to decompose all the remaining organic binders. Finally, controlled cracks were formed at the patterned edges depending on the conditions.

FEM Analysis. Conventional finite element method (FEM) software [COMSOL Multiphysics v. 5.6, structural mechanics module, physics-controlled mesh (basic auto mesh)] was used to simulate the deforming shapes of the wet TiO_2 paste after shrinkage. The structure was designed in a three-dimensional (3D) shape by using 3D Max and imported into COMSOL. The isotropic solid model of a linear elastic material in the solid mechanics module was used for the physics. We applied a strain of −20% to pyramid structures consisting of the wet TiO_2 paste and fixed them inside the structures patterned by the square shapes consisting of solidified TiO_2. The Poisson's ratio and Young's modulus of the wet TiO_2 paste material were set to 0.27 and 288 GPa, respectively. The geometry of the structures was the same as that of our pattern.

Characterization. The film thickness and crack formation were analyzed by scanning electron microscopy (SEM) using a field emission scanning electron microscope (JSM-6701F, JEOL) at an accelerating voltage of 10.0 kV. The NIH ImageJ program was used for image processing and analysis.

■ RESULTS

Figure 1a shows a schematic illustration of crack fragmentation in films imprinted with a micropyramid pattern when the residual film thickness is thick or thin compared to the size of a micropyramid. Flat wet TiO_2 colloidal films on a substrate were prepared by the doctor blade method with a commercial TiO_2 nanoparticle (NP) paste (18NR-T, Dyesol) containing organic compounds and ~20 nm TiO_2 NPs. We varied the thickness of the films by controlling the number and thickness of spacers during the doctor blade method. We prepared three micropyramidal PDMS molds with different widths (5 , 10, and 30 μm) replicated from masters (Figure S1), placed them on wet TiO_2 films, and applied slight pressure to fill the wet paste into the voids of the PDMS mold. Then, we annealed the sample at 60 °C to remove the solvent and detach the PDMS mold from the dried TiO_2 film. To remove all the organics

https://doi.org/10.1021/acs.langmuir.2c00328
Langmuir 2022, 38, 4935−4941

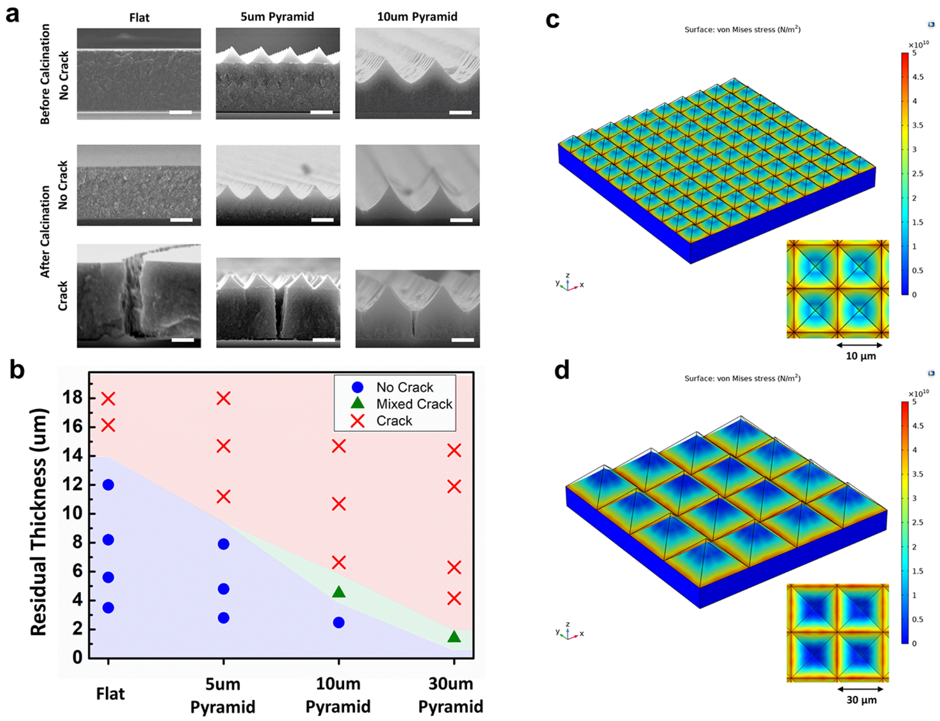

Figure 2. (a) Cross-sectional SEM images of crack generation in films with different residual thicknesses for flat, 5 μm square pyramid and 10 μm square pyramid TiO_2. The scale bars indicate 5 μm. (b) Diagram of the relationship between the film pattern and the residual layer thickness in crack generation. The stress distribution as a result of volume shrinkage of the paste during the sintering step was simulated for different micropattern sizes of (c) 10 and (d) 30 μm.

remaining in the film, TiO_2 films with solidified micropyramidal structures were calcinated at 500 °C. During the calcination process, the sharp edges of the pyramids played the role of notches to generate cracking. When the film thickness was approximately 12 μm (a relatively thin film thickness compared to the pyramid height), all pyramidal fragments were separated by controlled cracking (Figure 1b) because cracks propagated at all the notches. When the film thickness was approximately 34 μm (a relatively thick film thickness), however, cracks propagated only at some of the notches, and large rectangular fragments consisting of multiple pyramids were generated (Figure 1c).

In our system, there were two processes resulting in tensile stress, namely, the annealing process for the removal of the solvent at 60 °C and the calcination process at 500 °C, in which volume shrinkage occurred due to the elimination of all the organic compounds. To understand the mechanisms, we conducted thermogravimetric analysis (TGA). During the annealing process (60 °C), a weight loss of ~64% occurred (Figure S2a,b) due to the evaporation of most of the residual solvent in the paste. In the solidified film obtained after the annealing process, no cracks were observed because the PDMS mold held the TiO_2 paste and prevented the deformation of the pattern. Instead, crack initiation notches at the edges of the pyramid patterns were produced in both thin (Figure S3a,c) and thick (Figure S3b,d) films. During the calcination step, the remaining organics were completely eliminated, causing a weight loss of ~40% (Figure S2a,b) and a volume shrinkage of ~20% in the film (Figure S2c). We assume a shrinkage of ~20% as the strain for the generation of the cracks. The volume contraction in the open condition triggered crack propagation at the notches, although the degree of crack-induced fragmentation varied and was a function of film thickness. Note that we performed the experiments under two conditions. First, a thin TiO_2 film (~100 nm) was coated on the wafer as an adhesion promoter between the silicon wafer and the TiO_2 paste to ensure a no-slip boundary condition between the substrate and the film during cracking. Second, we coated the TiO_2 paste multiple times to obtain a high thickness to ensure film uniformity. When we tried to coat a thick film (thicker than 20 μm) in one application, the thickness in the edge area was much higher than that in the center region. We coated a thin TiO_2 layer using a doctor blade and removed the solvent at 60 °C for 90 min without placing a PDMS mold on the paste. We added a spacer to increase the thickness, and then we applied a TiO_2 paste coating again. We repeated the process to obtain the desired thickness. The relationship between the thickness and the spacer combination is summarized in Table S1.

While the colloidal film was being dried, the solvent-air menisci created capillary pressure on the top of the film during solvent evaporation. At the same time, volume shrinkage of the film occurred during calcination, leading to the development of tensile stresses in the film. These tensile stresses were released by crack generation when the film thickness exceeded the critical cracking thickness.[39−41] To investigate the effects of the notch and the size of the pyramid patterns on cracking, we conducted experiments on the cracking of films without patterns and with pyramid patterns of two different sizes. Figure 2a shows cross-sectional SEM images of a flat film and films imprinted with pyramidal shapes of two sizes (5 and 10 μm in period). The flat film is stable when the film thickness is 12.2 μm and cracks when the film thickness is increased to 16.0 μm. In the case of a film imprinted with pyramidal shapes, the film is not cracked when the residual thickness is 7.9 μm (5 μm in period) and 2.5 μm (10 μm in period) and cracked when

https://doi.org/10.1021/acs.langmuir.2c00328
Langmuir 2022, 38, 4935−4941

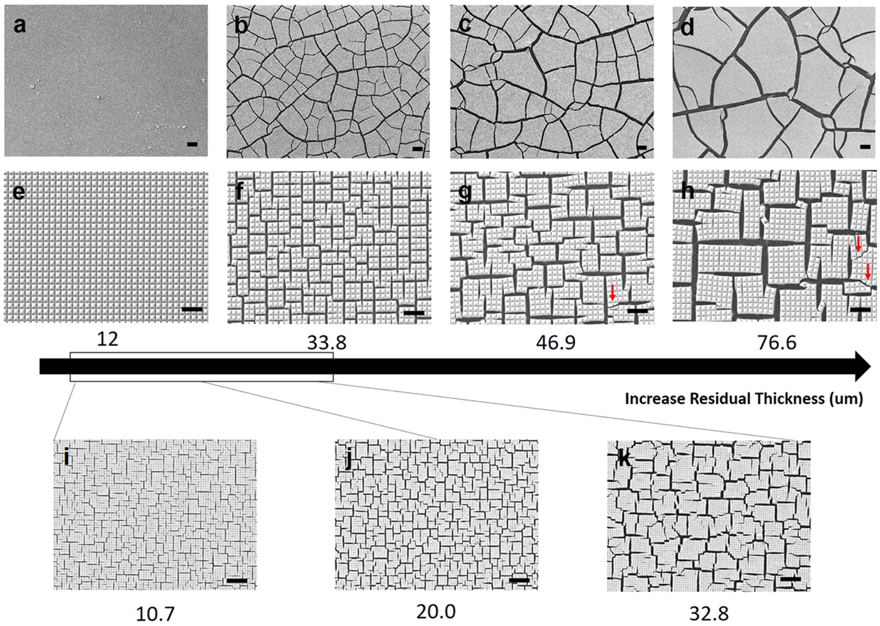

Figure 3. SEM images of flat TiO_2 films without crack initiation tips and micropatterned films with crack initiation tips consisting of square pyramids of two sizes (10 and 30 μm) after cracking at different residual layer thicknesses: for flat, (a) ~12, (b) ~34, (c) ~47, and (d) ~77 μm; for 30 μm micropatterned pyramids, (e) ~12, (f) ~34, (g) ~47, and (h) ~78 μm; and for 10 μm micropatterned pyramids, (i) ~11, (j) ~20, and (k) ~33 μm. The scale bars indicate 100 μm.

the residual thickness is 11.2 μm (5 μm in period) and 6.6 μm (10 μm in period), as shown in Figure 2a. The cracking events versus the residual thickness are plotted as a function of the pyramid pattern size in Figure 2b. The stress caused by volume shrinkage occurs randomly throughout the flat film, and cracks start to be generated at random positions above a film thickness of ~16 μm. However, in the micropyramid patterned films, the stress localizes at the edges of the pyramid pattern, and the strain energy required for crack generation is reduced due to stress localization. As a result, a relatively thin film thickness (~11.2 μm residual layer thickness for 5 μm micropyramid patterned films) is sufficient to generate cracks. When the pyramid period is increased to 10 μm, the critical thickness further decreases, as shown in Figure 2a,b. Cracks are generated when the residual layer thickness is ~6.6 μm, which is much lower than the critical thickness when the film is imprinted with 5 μm micropyramid patterns.

We analyzed the stress localization on pyramid patterns of different sizes with FEM simulations (Figure 2c,d). The stress is localized on the pyramid edges, which are notches, and it increases as the size of the pyramid increases. We note that the notch angle of pyramids with a width of 10 μm is slightly sharper (86°) than that of pyramids with a width of 30 μm (92°), which means that the size effect is high enough to overcome the notch effect. When the residual thickness is much higher than the critical thickness for cracking, the stress accumulation in the film is higher than the stress localization. Figure 3a−d shows the experimental results of fragmentation without the formation of crack initiation notches for various film thicknesses. When the residual film thickness is ~12 μm, no cracks are observed in the films after the calcination process (Figure 3a). The flat film is cracked at random and divided into small polygons of various sizes at a film thickness of ~34 μm (Figure 3b). The sizes of the polygons increase as the film thickness increases to ~47 μm (Figure 3c) and ~77 μm (Figure 3d). When we formed crack initiation tips by soft lithography with micropyramid patterns, cracks propagated in the horizontal or vertical direction, and rectangular fragments were obtained. Figure 3e−h shows the formation of rectangular fragments by cracking at various film thicknesses when using a 30 μm pyramidal mold. When the residual film thickness is ~12 μm, every notch (the valley between pyramids) propagates, creating cracks, during the calcination step, and the cracks divide pyramids one-by-one (1 × 1 blocks) (Figures 3e and S4a). Cracks are partially generated at the notches between the film thicknesses of ~12 μm and ~20 μm (Figure S4b). When the film thickness is increased from ~34 μm (Figure 3f) to ~78 μm (Figure 3h), the size of the rectangular fragments is also increased (Figure 3f−h). We note that some cracks propagate out of the lattice when the film thickness is higher than 47 μm (red arrows in Figure 3g,h). A similar phenomenon is observed when the size of the micropyramid pattern is reduced to 10 μm, but multiple pyramids are separated by cracks at a lower residual layer thickness. When the film thickness is increased from ~10.7 μm (Figure 3i) to ~32.8 μm (Figure 3k), the size of the rectangular fragments increases (Figure 3i−k).

We obtained the fragment area (A) from the image analysis program after conversion into black-and-white representations, as shown in Figure 4a−h. The calculated average areas for each film thickness were 24,708, 42,822, and 90,906 μm^2 for fragments consisting of polygons; 4609, 7602, and 20,676 μm^2 for fragments consisting of 30 μm multiple pyramids; and 890, 1443, and 4532 μm^2 for fragments consisting of 10 μm multiple pyramids, respectively. Figure 4i−k shows SEM images of cracked films with various coating thicknesses without any prepattern. The average crack spacing increases from 14.1 to 21.0 and 25.8 μm when the film thickness increases from 33.8 to 46.9 and 72.1 μm, respectively. Because the orientation of cracks is random, the standard deviation of the spacings is large (4.3−9.2 μm). In the case of the formation of tips by imprinting micropyramids, the cracks are straight and

https://doi.org/10.1021/acs.langmuir.2c00328
Langmuir 2022, 38, 4935−4941

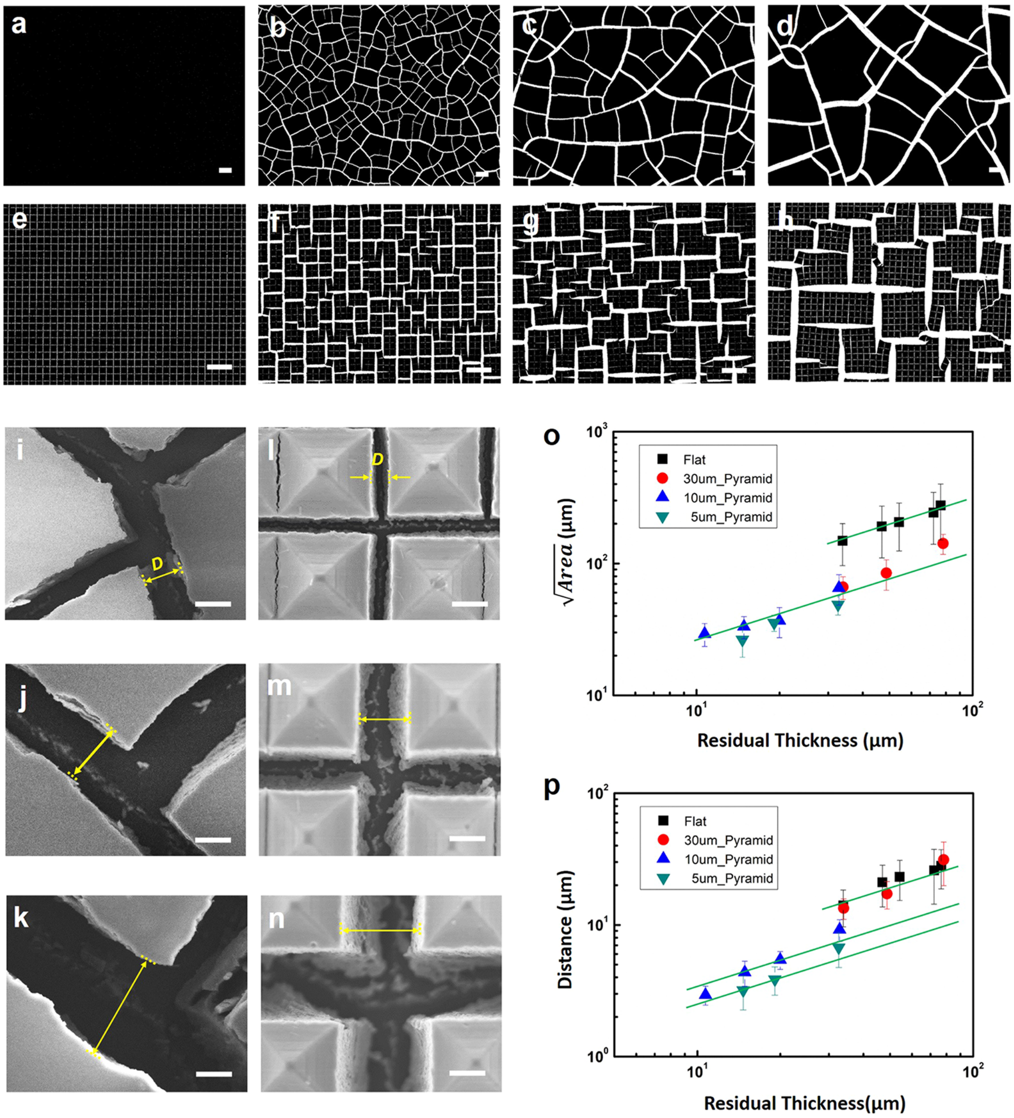

Figure 4. Black and white images of each figure were converted using image analysis software for films in different residual layer thicknesses: for flat, (a) ∼12, (b) ∼34, (c) ∼47, and (d) ∼77 μm and for micropatterned pyramids, (e) ∼12, (f) ∼34, (g) ∼47, and (h) ∼78 μm. The scale bars indicate 100 μm. The SEM images show the spacing between cracked fragments at different film thicknesses: for flat, (i) ∼33.8, (j) ∼46.9, and (k) ∼72.1 μm and for micropatterned pyramids, (l) ∼12.0, (m) ∼33.9, and (n) ∼78.2 μm. The scale bars indicate 10 μm. (o) Plot of the fragment area ($\sqrt{A}$) vs film thickness. (p) Plot of the spacing between fragments as a function of film thickness. The green lines show a slope of 2/3.

easier to measure. The SEM images shown in Figure 4l−n represent the crack spacings when the film has pyramid prepatterns. The average crack spacings with 30 μm pyramid patterns are 4.3, 11.1, and 21.9 μm when the film thickness is 12.0, 33.9, and 78.2 μm, respectively. In the case of the pyramidal shape, the cracks are controlled, and the standard deviation of the cracks is reduced to 1.1−7.1 μm. In addition, the average crack spacings with 10 μm pyramid patterns are 2.9, 4.3, 5.4, and 9.2 μm when the film thickness is 10.7, 14.8, 19.9, and 32.8 μm, respectively. When the size of the pyramid pattern is reduced, the standard deviation of the cracks is further reduced to 0.5−1.7 μm.

To discuss the relationship between the cracked area and the film thickness, we investigated the relationship between the fragment area (A) and the film thickness (h) (Figure 4o). The plot of the square root of the average fragment area ($A^{1/2}$) for all the experimental conditions and the film thickness (h) shows a linear relationship. The line in Figure 4o shows the scaling relationship between the cracked area and the film thickness in a flat film, $A \sim h^{4/3}$, which was reported as the scaling relation in drying films.[31,32] As shown in Figure 4o, the scaling relation between the fragment area and the film thickness is in good agreement with the experimental results. In the case of the relationship between the spacing and the film thickness, we assumed that the strain (ε) is constant in all the directions as follows

$$\frac{a_0 - a}{a_0} = \varepsilon = \text{constant} \tag{1}$$

a_0 and a are the length of the side of a fragment before and after cracking, respectively. The spacing (D) is the change in the fragment size during cracking, and the length is the square root of the area when the fragment is square.

$$D = 2(a_0 - a) = 2\varepsilon a_0 = 2\varepsilon\sqrt{A_0} \sim h^{2/3} \tag{2}$$

https://doi.org/10.1021/acs.langmuir.2c00328
Langmuir 2022, 38, 4935−4941

Figure 4p shows the relationship between the spacing and the film thickness, and the experimental results also follow the derived scaling relation. We note that the scaling results, even for rectangular fragments, can be strong evidence of the relationship between the fragment size and the film thickness.

■ CONCLUSIONS

We cracked colloidal films into rectangular fragments consisting of square pyramids. In this study, we examined the effect of notches and the thicknesses on the generation of cracks. Notches can guide crack initiation by stress localization, and the increase in thicknesses showed the effect of the mitigation of the notch effect. Under thin film thickness conditions, crack propagation occurs at all the notches, resulting in single, separate pyramids because the stress localization is dominant. Under thick film thickness conditions, the accumulation of film stress overcomes the stress localization, and only some of the notches can work for cracking. This can generate large rectangular fragments consisting of multiple pyramids. In our system, cracks in films with micropyramids are controllable and formed in straight lines, which is advantageous for measuring the size of the fragments and the crack spacing. Our cracking system with square pyramid patterns can provide a useful method for analyzing crack phenomena. Moreover, the system can provide a method for the preparation of controllable rectangular blocks in various sizes.

■ ASSOCIATED CONTENT

Supporting Information

The Supporting Information is available free of charge at https://pubs.acs.org/doi/10.1021/acs.langmuir.2c00328.

SEM images of pyramid pattern master; TGA results of the NP paste used in the present study; SEM images of the pyramid imprinted film before and after calcination with different film thicknesses; and relationship between the spacer and thickness (PDF)

■ AUTHOR INFORMATION

Corresponding Authors

Hyunsik Yoon − *Department of Chemical and Biomolecular Engineering, Seoul National University of Science and Technology, Seoul 01811, Republic of Korea*; orcid.org/0000-0002-6602-369X; Email: hsyoon@seoultech.ac.kr

Kookheon Char − *The National Creative Research Initiative Center for Intelligent Hybrids, The World Class University Program for Chemical Convergence for Energy and Environment, School of Chemical and Biological Engineering, Seoul National University, Seoul 08826, Republic of Korea*; orcid.org/0000-0002-7938-8022; Email: khchar@snu.ac.kr

Authors

Yunchan Lee − *The National Creative Research Initiative Center for Intelligent Hybrids, The World Class University Program for Chemical Convergence for Energy and Environment, School of Chemical and Biological Engineering, Seoul National University, Seoul 08826, Republic of Korea*

Jaekyoung Kim − *Department of Chemical and Biomolecular Engineering, Seoul National University of Science and Technology, Seoul 01811, Republic of Korea*

Soojin Lee − *The National Creative Research Initiative Center for Intelligent Hybrids, The World Class University Program for Chemical Convergence for Energy and Environment, School of Chemical and Biological Engineering, Seoul National University, Seoul 08826, Republic of Korea*

Sanghyuk Wooh − *School of Chemical Engineering & Materials Science, Chung-Ang University, Seoul 06974, Republic of Korea*; orcid.org/0000-0002-6535-370X

Complete contact information is available at: https://pubs.acs.org/10.1021/acs.langmuir.2c00328

Notes

The authors declare no competing financial interest.

■ ACKNOWLEDGMENTS

This work was supported by the National Creative Research Initiative Program for "Intelligent Hybrids Research Center" (no. 2010-0018290) funded by the Korea Ministry of Science, ICT and Future Planning (MSIP), a National Research Foundation of Korea grant, the BK21 Plus Program in SNU Chemical Engineering funded by the Ministry of Education, Science and Technology of Korea, and the Technology Innovation Program (20010371) funded by the Ministry of Trade, Industry and Energy (Korea).

■ REFERENCES

(1) Kindle, E. M. Some Factors Affecting the Development of Mud-Cracks. *J. Geol.* **1917**, *25*, 135−144.

(2) Bucklow, S. L. A Stylometric Analysis of Craquelure. *Comput. Humanities* **1997**, *31*, 503−521.

(3) Bohn, S.; Platkiewicz, J.; Andreotti, B.; Adda-Bedia, M.; Couder, Y. Hierarchical Crack Pattern as Formed by Successive Domain Divisions. II. From Disordered to Deterministic Behavior. *Phys. Rev. E* **2005**, *71*, 046215.

(4) Milinkovitch, M. C.; Manukyan, L.; Debry, A.; Di-Poï, N.; Martin, S.; Singh, D.; Lambert, D.; Zwicker, M. Crocodile Head Scales Are Not Developmental Units But Emerge from Physical Cracking. *Science* **2013**, *339*, 78−81.

(5) Lee, W. P.; Routh, A. F. Why Do Drying Films Crack? *Langmuir* **2004**, *20*, 9885−9888.

(6) Tirumkudulu, M. S.; Russel, W. B. Cracking in Drying Latex Films. *Langmuir* **2005**, *21*, 4938−4948.

(7) Choi, Y. W.; Kang, D.; Pikhitsa, P. V.; Lee, T.; Kim, S. M.; Lee, G.; Tahk, D.; Choi, M. Ultra-Sensitive Pressure Sensor Based on Guided Straight Mechanical Cracks. *Sci. Rep.* **2017**, *7*, 40116.

(8) Ahn, C.-Y.; Jang, S.; Cho, Y.-H.; Choi, J.; Kim, S.; Kim, S. M.; Sung, Y.-E.; Choi, M. Guided Cracking of Electrodes by Stretching Prism-Patterned Membrane Electrode Assemblies for High-Performance Fuel Cells. *Sci. Rep.* **2018**, *8*, 1257.

(9) Qin, Z.; Pugno, N. M.; Buehler, M. J. Mechanics of Fragmentation of Crocodile Skin and Other Thin Films. *Sci. Rep.* **2014**, *4*, 4906.

(10) Halász, Z.; Nakahara, A.; Kitsunezaki, S.; Kun, F. Effect of Disorder on Shrinkage-Induced Fragmentation of a Thin Brittle Layer. *Phys. Rev. E* **2017**, *96*, 033006.

(11) Zhang, J.; Lu, Y.; He, L.; Yang, L.; Ni, Y. Modeling Progressive Interfacial Debonding of a Mud-Crack Film on Elastic Substrates. *Eng. Fract. Mech.* **2017**, *177*, 123−132.

(12) Prosser, J. H.; Brugarolas, T.; Lee, S.; Nolte, A. J.; Lee, D. Avoiding Cracks in Nanoparticle Films. *Nano Lett.* **2012**, *12*, 5287−5291.

(13) Lama, H.; Mondal, R.; Basavaraj, M. G.; Satapathy, D. K. Cracks in Dried Deposits of Hematite Ellipsoids: Interplay Between Magnetic and Hydrodynamic Torques. *J. Colloid Interface Sci.* **2018**, *510*, 172−180.

(14) Domokos, G.; Kun, F.; Sipos, A. Á.; Szabó, T. Universality of Fragment Shapes. *Sci. Rep.* **2015**, *5*, 9147.
(15) Goehring, L.; Conroy, R.; Akhter, A.; Clegg, W. J.; Routh, A. F. Evolution of Mud-Crack Patterns During Repeated Drying Cycles. *Soft Matter* **2010**, *6*, 3562−3567.
(16) Seghir, R.; Arscott, S. Controlled Mud-Crack Patterning and Self-Organized Cracking of Polydimethylsiloxane Elastomer Surfaces. *Sci. Rep.* **2015**, *5*, 14787.
(17) Smith, M. I.; Sharp, J. S. Effects of Substrate Constraint on Crack Pattern Formation in Thin Films of Colloidal Polystyrene Particles. *Langmuir* **2011**, *27*, 8009−8017.
(18) Yow, H. N.; Goikoetxea, M.; Goehring, L.; Routh, A. F. Effect of Film Thickness and Particle Size on Cracking Stresses in Drying Latex Films. *J. Colloid Interface Sci.* **2010**, *352*, 542−548.
(19) Leung, K.-T.; Józsa, L.; Ravasz, M.; Néda, Z. Pattern Formation—Spiral Cracks Without Twisting. *Nature* **2001**, *410*, 166.
(20) Lazarus, V.; Pauchard, L. From Craquelures to Spiral Crack Patterns: Influence of Layer Thickness on the Crack Patterns Induced by Desiccation. *Soft Matter* **2011**, *7*, 2552−2559.
(21) Rao, K. D. M.; Gupta, R.; Kulkarni, G. U. Fabrication of Large Area, High-Performance, Transparent Conducting Electrodes Using a Spontaneously Formed Crackle Network as Template. *Adv. Mater. Interfaces* **2014**, *1*, 1400090.
(22) Zeid, W. B.; Brutin, D. Influence of Relative humidity on Spreading, Pattern Formation and Adhesion of a Drying Drop of Whole Blood. *Colloids Surf., A* **2013**, *430*, 1−7.
(23) Sobac, B.; Colinet, P.; Pauchard, L. Influence of Benard-Marangoni Instability on the Morphology of Drying Colloidal Films. *Soft Matter* **2019**, *15*, 2381−2390.
(24) Sun, W.; Jia, F.; Sun, Z.; Zhang, J.; Li, Y.; Zhang, X.; Yang, B. Manipulation of Cracks in Three-Dimensional Colloidal Crystal Films via Recognition of Surface Energy Patterns: An Approach to Regulating Crack Patterns and Shaping Microcrystals. *Langmuir* **2011**, *27*, 8018−8026.
(25) Baëtens, T.; Pallecchi, E.; Thomy, V.; Arscott, S. Cracking effects in squashable and stretchable thin metal films on PDMS for flexible microsystems and electronics. *Sci. Rep.* **2018**, *8*, 9492.
(26) Ma, J.; Jing, G. Possible Origin of the Crack Pattern in Deposition Films Formed from a Drying Colloidal Suspension. *Phys. Rev. E* **2012**, *86*, 061406.
(27) Phillips, K. R.; Zhang, C. T.; Yang, T.; Kay, T.; Gao, C.; Brandt, S.; Liu, L.; Yang, H.; Li, Y.; Aizenberg, J.; Li, L. Fabrication of Photonic Microbricks via Crack Engineering of Colloidal Crystals. *Adv. Funct. Mater.* **2020**, *30*, 1908242.
(28) Wooh, S.; Lee, S.; Lee, Y.; Ryu, J. H.; Lee, W. B.; Yoon, H.; Char, K. Isolated Mesoporous Microstructures Prepared by Stress Localization-Induced Crack Manipulation. *ACS Nano* **2016**, *10*, 9259−9266.
(29) Allain, C.; Limat, L. Regular Patterns of Cracks Formed by Directional Drying of a Colloidal Suspension. *Phys. Rev. Lett.* **1995**, *74*, 2981−2984.
(30) Groisman, A.; Kaplan, E. An Experimental-Study of Cracking Induced by Desiccation. *Europhys. Lett.* **1994**, *25*, 415−420.
(31) Ma, X.; Lowensohn, J.; Burton, J. C. Universal Scaling of Polygonal Desiccation Crack Patterns. *Phys. Rev. E* **2019**, *99*, 012802.
(32) Cho, H. J.; Datta, S. S. Scaling Law for Cracking in Shrinkable Granular Packings. *Phys. Rev. Lett.* **2019**, *123*, 158004.
(33) Leung, K.-t.; Néda, Z. Pattern Formation and Selection in Quasistatic Fracture. *Phys. Rev. Lett.* **2000**, *85*, 662−665.
(34) Sadhukhan, S.; Kumar, A.; Kulkarni, G. U.; Tarafdar, S.; Dutta, T. A Spring Network Simulation in Three Dimensions for Designing Optimal Crack Pattern Template to Fbricate Transparent Conducting Electrodes. *B. Mater. Sci.* **2019**, *42*, 197.
(35) Flores, J. C. Mean-Field Crack Networks on Desiccated Films and Their Applications: Girl with a Pearl Earring. *Soft Matter* **2017**, *13*, 1352−1356.
(36) Iqbal, R.; Shen, A. Q.; Sen, A. K. Understanding of the Role of Dilution on Evaporative Deposition Patterns of Blood Droplets over Hydrophilic and Hydrophobic Substrates. *J. Colloid Interface Sci.* **2020**, *579*, 541−550.
(37) Chen, R.; Zhang, L.; Zang, D.; Shen, W. Understanding Desiccation Patterns of Blood Sessile Drops. *J. Mater. Chem. B* **2017**, *5*, 8991−8998.
(38) Wooh, S.; Koh, J. H.; Lee, S.; Yoon, H.; Char, K. Trilevel-Structured Superhydrophobic Pillar Arrays with Tunable Optical Functions. *Adv. Funct. Mater.* **2014**, *24*, 5550−5556.
(39) Dufresne, E. R.; Corwin, E. I.; Greenblatt, N. A.; Ashmore, J.; Wang, D. Y.; Dinsmore, A. D.; Cheng, J. X.; Xie, X. S.; Hutchinson, J. W.; Weitz, D. A. Flow and Fracture in Drying Nanoparticle Suspensions. *Phys. Rev. Lett.* **2003**, *91*, 224501.
(40) Dufresne, E. R.; Stark, D. J.; Greenblatt, N. A.; Cheng, J. X.; Hutchinson, J. W.; Mahadevan, L.; Weitz, D. A. Dynamics of Fracture in Drying Suspensions. *Langmuir* **2006**, *22*, 7144−7147.
(41) Jagla, E. A. Stable Propagation of an Ordered Array of Cracks During Directional Drying. *Phys. Rev. E* **2002**, *65*, 046147.

https://doi.org/10.1021/acs.langmuir.2c00328
Langmuir 2022, 38, 4935−4941